Transient Simulation Technique for HVDC Systems

Yongnam Cho, Student Member, IEEE, George J. Cokkinides, Senior Member, IEEE, and
A.P. Meliopoulos, Fellow, IEEE

Abstract--**This paper presents an advanced transient simulation method, the quadratic integration method, and its application to the simulation of HVDC systems. The quadratic integration method demonstrates several superior features that ensure higher fidelity and stability in transient analysis of systems with nonlinearities and switching subsystems: nonlinear model equations are converted into a set of linear and quadratic equation with the introduction of new variables (model quadratization) and the resulting equations are integrated assuming a quadratic variation over the integration time step (quadratic integration). The method eliminates fictitious oscillations exhibited by trapezoidal integration. Furthermore, the quadratic integration method is more accurate and robust than trapezoidal integration and other transient analysis tools.**

In this paper, the superior properties of the quadratic integration in power system transient analysis are demonstrated by comparing the quadratic integration with the trapezoidal integration in the simulation of High Voltage Direct Current (HVDC) system with switching subsystems and nonlinear components.

Keywords: **Quadratic integration, numerical method, transient simulation, numerical oscillation, 12-pulse converter, equidistant control, nonlinear transformer.**

I. INTRODUCTION

S INCE the demands for utilizing long distant sources, and linking different frequency systems have been increasing, HVDC transmission systems, are becoming one of the most promising technologies to meet the need for reliable and cost effective transmission. Specially, the rapid increase of wind power in remote locations has accelerated the necessity of more advanced, reliable and cost effective applications of HVDC transmission systems. High fidelity transient simulation technique can be a useful tool for the advanced design and optimization of HVDC transmission systems with nonlinearities and switching subsystems.

Numerical integration methods have been extensively studied and applied to transient analysis of power systems with nonlinear and switching components. The most predominant method among the time domain transient simulation methods is trapezoidal integration due to its property of absolute stability (A-stable) [1],[2]. However, the trapezoidal integration is problematic when applied to network systems with nonlinearities and switching subsystems. Fictitious oscillations can be generated, when the state of the network model suddenly changes. The fictitious oscillations can be also shown at certain combinations of integration time step and system natural frequencies. Therefore, the system model with nonlinearities and switching subsystems cannot be analyzed properly by pure application of the trapezoidal integration. Additional algorithmic controls are needed for the trapezoidal integration, when it is used in systems with nonlinearities and power electronics (switching systems). Specifically, in order to suppress the numerical oscillations of the trapezoidal method, several approaches have been proposed, such as numerical stabilizer method [3], (b) critical damping adjustment (CDA)[4],[5], and (c) wave digital filter (WDF)[2],[6]. Numerical stabilizers slightly change both the structure and the state equations of the network model, and cannot flawlessly eliminate fictitious oscillation. The CDA method requires variable time step. Variable time step requires that the companion matrices of all devices must be recomputed for critical conditions, and the sampling rate during critical conditions is higher of that during standard conditions. The WDF method can generate some distortions. The distortions may be problematic in some cases, leading to less accurate results.

The quadratic integration method has been introduced to eliminate fictitious oscillations exhibited by the application of the trapezoidal integration, and enhance simulation accuracy. Since the method has a natural characteristic to eliminate fictitious oscillation, additional algorithmic controls to suppress numerical oscillation is not needed. The quadratic integration method is highly robust and stable.

In this paper, the properties of the quadratic integration are compared to the trapezoidal integration, and the method is demonstrated on a typical 12-pulse HVDC system, using nonlinear transformer models and 12-pulse converters.

II. DESCRIPTION OF QUADRATIC INTEGRATION

The quadratic integration is based on two concepts: (a) nonlinear equations of systems are reformulated into either linear or quadratic equations by the introduction of additional state variables, and (b) the resulting equations are integrated assuming that the equations vary quadratically over the time period of one time step. The quadratic integration method performs better in terms of both stability and accuracy. These properties ensure that HVDC systems with nonlinear components and switching subsystems can be modeled, and simulated with greater accuracy.

The quadratic integration method is a special case of a class of methods known as collocation methods [1]. As shown in Fig. 1, the method has three collocation points at $x(t-h)$, $x(t-h/2)$, and $x(t)$ in the integration time interval [t-h,t].

Yongnam Cho, George J. Cokkinides, A.P Meliopoulos are with the School of Electrical and Computer Engineering , Georgia Institute of Technology, Atlanta, GA,30332 USA (e-mail: ycho8@mail.gatech.edu, George.cokkinides@ece.gatech.edu, sakis.m@gatech.edu).
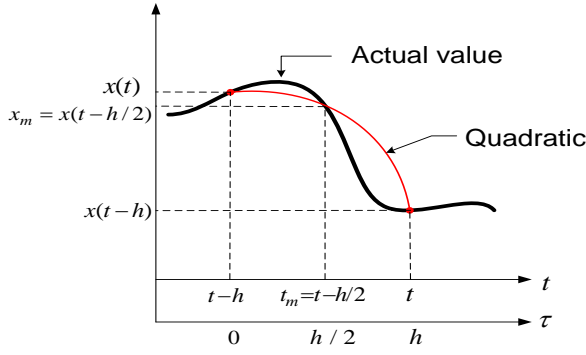
Fig. 1. Graphical illustration of quadratic integration

Assuming that the function $x(t)$, as shown in Fig.1, varies quadratically in the interval $[t\text{-}h,\ t]$, i.e. $x(\tau) = a + b\tau + c\tau^2$, the three parameters a, b, and c can be expressed as a function of the three collocation points. The result is:

$$a = x(t-h),\ b = \frac{1}{h}\left(-3x(t-h) + 4x_m - x(t)\right),\ \text{and}$$

$$c = \frac{2}{h^2}\left(x(t-h) - 2x_m + x(t)\right),$$

where x_m is the value x at the mid-point, i.e. at time $t\text{-}h/2$.
Then, the integration of the quadratic function is straightforward.
The procedure will be illustrated with a simple differential

equation: $\dfrac{dx(t)}{dt} = Ax(t)$ (1)

Equation (1) is integrated from t-h to t and from t-h to t-h/2, yielding:

$$x(t) - x(t-h) = A \cdot \int_{t-h}^{t} x(\tau)d\tau,\ \text{and}$$

$$x_m - x(t-h) = A \cdot \int_{t-h}^{t-h/2} x(\tau)d\tau. \tag{2}$$

Upon evaluation of the integrals and rearranging the following matrix equation is obtained (algebraic companion form) that can be applied repetitively to provide the solution to the differential equation:

$$\begin{bmatrix} \dfrac{h}{24}A & I - \dfrac{h}{3}A \\ I - \dfrac{h}{6}A & -\dfrac{2h}{3}A \end{bmatrix} \cdot \begin{bmatrix} x(t) \\ x_m \end{bmatrix} = \begin{bmatrix} \left(I + \dfrac{5h}{24}A\right) \\ \left(I + \dfrac{h}{6}A\right) \end{bmatrix} \cdot x(t-h) \tag{3}$$

As another example, consider the following form of a power device model (as a set of differential equations):

$$\begin{bmatrix} i(t) \\ 0 \end{bmatrix} = A \cdot \begin{bmatrix} v(t) \\ y(t) \end{bmatrix} + B \cdot \frac{d}{dt}\begin{bmatrix} v(t) \\ y(t) \end{bmatrix} \tag{4}$$

where $i(t) = \begin{bmatrix} i_1(t) & i_2(t) & \dots & i_{m-1}(t) & i_m(t) \end{bmatrix}^T$,

$v(t) = \begin{bmatrix} v_1(t) & v_2(t) & \dots & v_{k-1}(t) & v_k(t) \end{bmatrix}^T$,

$y(t) = \begin{bmatrix} y_1(t) & y_2(t) & \dots & y_{p-1}(t) & y_p(t) \end{bmatrix}^T$,

A and B are $n \times n$ matrices, $n = p + k$, and $y(t)$ is internal state variables.
The algebraic companion form in the time interval is represented as (5).

$$C\begin{bmatrix} i(t) \\ 0 \\ i(t_m) \\ 0 \end{bmatrix} = D\begin{bmatrix} v(t) \\ y(t) \\ v(t_m) \\ y(t_m) \end{bmatrix} - E\begin{bmatrix} v(t-h) \\ y(t-h) \end{bmatrix} - F\begin{bmatrix} i(t-h) \\ 0 \end{bmatrix} \tag{5}$$

where: $i(t_m) = \begin{bmatrix} i_1(t_m) & i_2(t_m) & \dots & i_{m-1}(t_m) & i_m(t_m) \end{bmatrix}$,

$v(t_m) = \begin{bmatrix} v_1(t_m) & v_2(t_m) & \dots & v_{k-1}(t_m) & v_k(t_m) \end{bmatrix}$,

$y(t_m) = \begin{bmatrix} y_1(t_m) & y_2(t_m) & \dots & y_{p-1}(t_m) & y_p(t_m) \end{bmatrix}$,

$$C = \begin{bmatrix} -\dfrac{h}{24}C_I & \dfrac{h}{3}C_I \\ \dfrac{h}{6}C_I & \dfrac{2h}{3}C_I \end{bmatrix},\ D = \begin{bmatrix} -\dfrac{h}{24}A & \dfrac{h}{3}A + B \\ \dfrac{h}{6}A + B & \dfrac{2h}{3}A \end{bmatrix}$$

$$E = \begin{bmatrix} -\dfrac{5h}{24}A + B \\ -\dfrac{h}{6}A + B \end{bmatrix},\ F = \begin{bmatrix} \dfrac{5h}{24}C_I \\ \dfrac{h}{6}C_I \end{bmatrix},\ C_I = \begin{bmatrix} 1 & 0 & \cdots & 0 & 0 \\ 0 & 1 & 0 & 0 & 0 \\ \vdots & 0 & 0 & 0 & 0 \\ 0 & 0 & 0 & 0 & 0 \\ 0 & 0 & 0 & 0 & 0 \end{bmatrix}$$

where t_m is the mid-point of the integration time step $[t\text{-}h,\ t]$.
Standard nodal analysis methods are used to obtain the network equations from the component algebraic companion forms in the same way as in the trapezoidal integration method. Except in this case, nodal equations are written for both time t and $t\text{-}h/2$ resulting in twice as many network equations as in the trapezoidal integration.

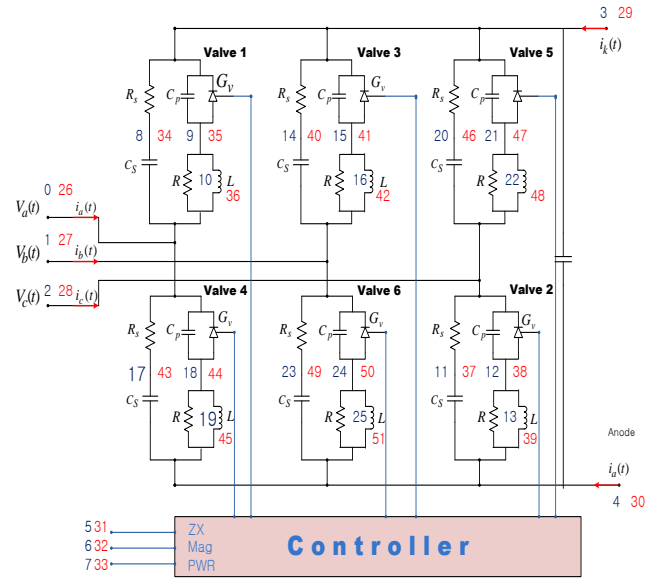## DESCRIPTION OF 6-PULSE CONVERTER AND NONLINEAR TRANSFORMER

Fig. 2. A six-pulse converter model.

This section presents a generalized methodology for modeling the HVDC system, based on modules of 6-pulse converters, three phase saturable core transformers, transmission lines and three phase sources. These devices are modeled with a set of nonlinear and differential equations derived directly from the physical parameters. Application of quadratic integration leads to an algebraic companion form in

terms of voltages and currents at two future points in time.

A. 6-pulse Converter Model

The 6-pulse converter consists of six single valves (with snubber circuits and current limiting reactors) and a smoothing capacitor as shown in Fig.2. The single valve and smoothing capacitor of Fig.3 is modeled and merged to formulate the topology of the six-pulse converter using standard nodal analysis method.
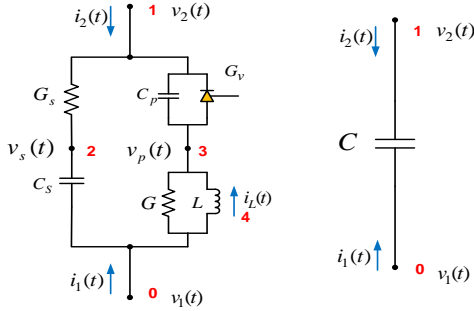
A single valve   A smoothing capacitor

Fig. 3. A single valve model and smoothing capacitor model.

The development of the algebraic companion forms for the two models of Fig. 3 are derived with the procedure described in the previous section. The resulting models are:
The algebraic companion form of the single valve is:

$$C_V \begin{bmatrix} i(t) \\ 0 \\ i(t_m) \\ 0 \end{bmatrix} = D_V \begin{bmatrix} v(t) \\ y_1(t) \\ v(t_m) \\ y_1(t_m) \end{bmatrix} - E_V \begin{bmatrix} v(t-h) \\ y_1(t-h) \end{bmatrix} - F_V \begin{bmatrix} i(t-h) \\ 0 \end{bmatrix} \quad (6)$$

where:

$i(t) = [i_1(t) \quad i_2(t)]$, $y(t) = [v_s(t) \quad v_p(t) \quad i_L(t)]$,

$v(t) = [v_1(t) \quad v_2(t)]$, $v(t_m) = [v_1(t_m) \quad v_2(t_m)]$,

$i(t_m) = [i_1(t_m) \quad i_2(t_m)]$, $y(t_m) = [v_s(t_m) \quad v_p(t_m) \quad i_L(t_m)]$,

$$C_I = \begin{bmatrix} 1 & 0 & 0 & 0 & 0 \\ 0 & 1 & 0 & 0 & 0 \\ 0 & 0 & 0 & 0 & 0 \\ 0 & 0 & 0 & 0 & 0 \\ 0 & 0 & 0 & 0 & 0 \end{bmatrix}, A = \begin{bmatrix} G & 0 & 0 & -G & 1 \\ 0 & G_S+G_V & -G_S & -G_V & 0 \\ 0 & -G_S & G_S & 0 & 0 \\ -G & -G_V & 0 & G+G_V & -1 \\ -1 & 0 & 0 & 1 & 0 \end{bmatrix},$$

$$\text{and } B = \begin{bmatrix} C_S & 0 & -C_S & 0 & 0 \\ 0 & C_P & 0 & -C_P & 0 \\ -C_S & 0 & C_S & 0 & 0 \\ 0 & -C_P & 0 & C_P & 0 \\ 0 & 0 & 0 & 0 & L \end{bmatrix}.$$

The algebraic companion form of the smoothing capacitor is:

$$C_{cap} \begin{bmatrix} i(t) \\ i(t_m) \end{bmatrix} = D_{cap} \begin{bmatrix} v(t) \\ v(t_m) \end{bmatrix} - E_{cap}[v(t-h)] - F_{cap}[i(t-h)] \quad (7)$$

where: $i(t) = [i_1(t) \quad i_2(t)]$, $v(t) = [v_1(t) \quad v_2(t)]$,

$i(t_m) = [i_1(t_m) \quad i_2(t_m)]$, $v(t_m) = [v_1(t_m) \quad v_2(t_m)]$,

$$C_s = \begin{bmatrix} 1 & 0 \\ 0 & 1 \end{bmatrix}, A = \begin{bmatrix} 0 & 0 \\ 0 & 0 \end{bmatrix}, \text{ and } B = \begin{bmatrix} -c & c \\ c & -c \end{bmatrix}.$$

TABLE I
VALVE POINTERS

valve #	States									
	External (t)		Internal(t) (t)			External (t_m)		Internal (t_m)		
1	0	3	8	9	10	26	29	34	35	36
2	4	2	11	12	13	30	28	37	38	39
3	1	3	14	15	16	27	29	40	41	42
4	4	0	17	18	19	30	26	43	44	45
5	2	3	20	21	22	28	29	46	47	48
6	4	1	23	24	25	30	27	49	50	51

TABLE II
SMOOTHING CAPACITOR POINTERS

Cap #	States			
1	3	4	29	30

The six-pulse converter model is formulated by connecting six single valves and a smoothing capacitor to specific nodes of a six-pulse converter. The specific nodes are defined on the six-pulse converter of Fig. 2. The state variables consist of internal states and external states, and are defined in terms of corresponding nodes. The algebraic companion form of the entire six-pulse converter is obtained by application of standard nodal analysis, i.e. the sum of currents at each node equals zero. Substitution using the algebraic companion form and casting the equations in a matrix form provides the 6-pulse converter model. This process is achieved with the algorithm below, and the connectivity pointers of Tables I and II.

DO WHILE ($iValve <$ Number of valve)
    DO WHILE ($i <$ Number of ROW)
        $i1 =$ Valve Pointer [i][$ivalve$]
        DO WHILE ($j <$ Number of Column)
            $j1 =$ Valve Pointer [j][$ivalve$]
            $A_{conv}[i1][j1] = A_v[i][j]$
            $B_{conv}[i1][j1] = B_v[i][j]$
            $C_{conv}[i1][j1] = C_v[i][j]$
            $D_{conv}[i1][j1] = D_v[i][j]$
        END DO
    END DO
  END DO
Where $i = 1, 2, ..., number\ of\ row\ of\ each\ matrix$, and
      $j = 1, 2, ..., number\ of\ column\ of\ each\ matrix$

The algebraic companion form of the six-pulse converter has the following form.

$$C_{con} \begin{bmatrix} i(t) \\ 0 \\ i(t_m) \\ 0 \end{bmatrix} = D_{con} \begin{bmatrix} v(t) \\ y_1(t) \\ v(t_m) \\ y_1(t_m) \end{bmatrix} - E_{con} \begin{bmatrix} v(t-h) \\ y_1(t-h) \end{bmatrix} - F_{con} \begin{bmatrix} i(t-h) \\ 0 \end{bmatrix} \quad (8)$$

where: $i(t) = [i_a(t) \quad i_b(t) \quad i_c(t) \quad i_{kd}(t) \quad i_{ad}(t)]^T$,

$$v(t) = \begin{bmatrix} v_a(t) & v_b(t) & v_c(t) & v_{kd}(t) & v_{ad}(t) \end{bmatrix}^T,$$

$$y(t) = \begin{bmatrix} y_1(t) & y_2(t) & y_3(t) & y_4(t) & y_5(t) & y_6(t) \end{bmatrix}^T,$$

$$i(t_m) = \begin{bmatrix} i_a(t_m) & i_b(t_m) & i_c(t_m) & i_{kd}(t_m) & i_{ad}(t_m) \end{bmatrix}^T,$$

$$v(t_m) = \begin{bmatrix} v_a(t_m) & v_b(t_m) & v_c(t_m) & v_{kd}(t_m) & v_{ad}(t_m) \end{bmatrix}^T,$$

$$y(t_m) = \begin{bmatrix} y_1(t_m) & y_2(t_m) & y_3(t_m) & y_4(t_m) & y_5(t_m) & y_6(t_m) \end{bmatrix}^T,$$

C_{conv} and D_{conv} are a 52 by 52 matrices, and E_{conv}, and F_{conv} are 52 by 26 matrices.

B. Three Phase Saturable Core Transformer

This section presents a method to quadratize nonlinear equations. An example of a single phase saturable transformer is used as it is illustrated in Fig.4.
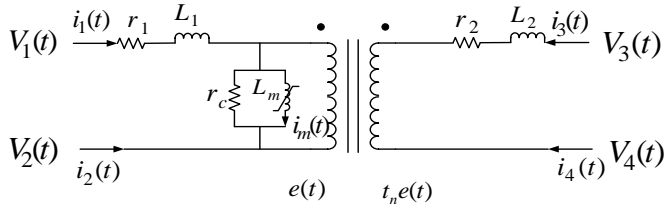
Fig. 4 A single phase saturable core transformer

The saturable core transformer is one of nonlinear components. The core magnetizing reactance is modeled as a nonlinear inductor with a (magnetizing) current that depends on the core flux via a highly nonlinear equation (9):

$$i_m(t) = i_0 \left| \frac{\lambda}{\lambda_0} \right|^n \cdot sign(\lambda(t)) \tag{9}$$

The exponent n is typically 9 to 11 for usual magnetic material used for transformers. The above equation can be quadratized by introducing additional states and corresponding equations. The number of additional states and equations depends on the nonlinearity (exponent n). For simplicity, we show below the application of this procedure in case the exponent is 5. This case requires the introduction of two additional states, i.e. z_1 and z_2, and two additional equations. The system equations for the single phase saturable transformer (including all equations, i.e. linear and quadratized equations) are as follows.

$$r_1 i_1(t) + L_1 \frac{d}{dt} i_1(t) = v_1(t) - v_2(t) - e(t) \tag{10}$$

$$i_1(t) + i_2(t) = 0 \tag{11}$$

$$r_2 i_3(t) + L_2 \frac{d}{dt} i_3(t) = v_3(t) - v_4(t) - t_n e(t) \tag{12}$$

$$i_3(t) + i_4(t) = 0 \tag{13}$$

$$r_c i_1(t) + r_c t i_3(t) = r_c i_m(t) + e(t) \tag{14}$$

$$o = e(t) - \frac{d}{dt} \lambda(t) \tag{15}$$

$$0 = i_m(t) - \frac{i_0}{\lambda_0} \lambda(t) z_2(t) \tag{16}$$

$$0 = z_2(t) - z_1^2(t) \tag{17}$$

$$0 = \lambda_0^2 \cdot z_1(t) - \lambda^2(t) \tag{18}$$

A compact matrix form consisting of quadratic equations and differential equations can be written for each phase of a three phase transformer. Quadratic integration will yield the algebraic companion form of the single phase transformer. Subsequently, the algebraic companion form of a single phase saturable transformer can be merged to form a three phase saturable transformer in the same process as that of the six pulse converter.

C. Control Action-Equidistant Control

The six-pulse converter can be controlled with a number of strategies. We have elected to use equidistant control. The digital controller for the equidistant control includes an estimator of control references, and the actual control in terms of equidistant valve firing pulses [8]-[12].

The control references consist of two parameters, magnitude and zero-crossing time of Line-Line voltage (V_{AB}) between phase A and phase B. Since HVDC systems contain several components with nonlinear characteristic, V_{AB} can be distorted by harmonics. For better accuracy of the control scheme reference, first the positive sequence of fundamental frequency is estimated by using Fourier analysis and modal decomposition and then the reference is computed (V_{ab1}).

For the equidistant control scheme, the firing delay angle (α) is used to control the switching sequence. The scheme of equidistant control is shown in Fig.5.
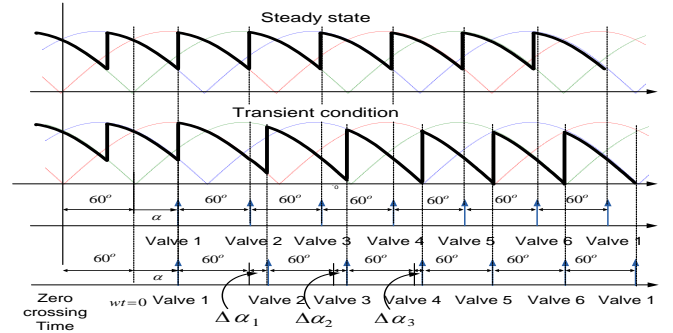

Fig. 5. Scheme of equidistant control for switching sequence

In steady state, the six firing signals for the six thyristors are generated, from the zero-crossing time, in equal intervals of 60^0 from each signal pulse. Since the HVDC systems are dynamic systems with their specific transient response to changes, such as power order changes, feeding power variations, and frequency variations, the firing delay angle has to be regulated, until the system reaches the steady state as shown in Fig.5. For the dynamic control of the six-pulse rectifier, the entire process to compute switching sequence is presented in Fig.6.
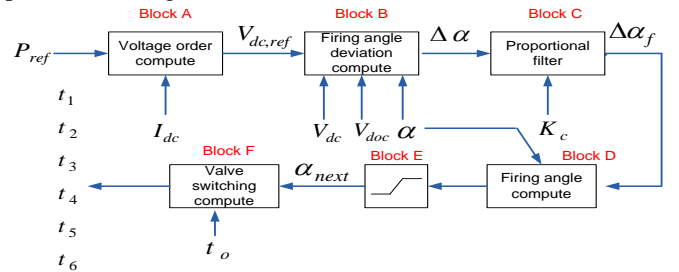

Fig. 6. Control scheme of the six-pulse rectifier

In Block A, a direct voltage reference of converter $V_{dc,ref}$ is

computed by dividing reference power P_{ref} into measured direct current I_{dc}. With the voltage reference, a deviation of firing angle $\Delta\alpha$ is calculated in Block B as follows:

$$V_{dc} = V_{d0c}\cos\alpha - K_{\Omega c}I_{dc} \qquad (19)$$

$$\Delta V = -V_{d0c}\sin\alpha \cdot \Delta\alpha , \qquad (20)$$

$$\Delta\alpha = \frac{\Delta V}{-V_{d0c}\sin\alpha} \qquad \Delta V = V_{ref} - V_{dc}. \qquad (21)$$

Where V_{dc} is the measured direct voltage, V_{d0c} is no-load direct voltage at converter side, and $K_{\Omega c}$ is the equivalent commutation resistance. It is obvious that the relationship between direct voltage and firing angle is inherently nonlinear as shown in (19). However, as shown in (21), the linear relation between the deviations of both firing angle and direct voltage exists, and the digital controller can linearly regulate the six-pulse converter. In the next Block $\Delta\alpha$ is proportionally filtered with $\Delta\alpha_f = K_c \cdot \Delta\alpha$, so that large changes (jumps) in firing angle are avoided and the digital controller can ensure smooth transitions and robust and stable operation. A new firing angle α_{next} is calculated in Block D by summing present firing angle and filtered deviation of firing angle, and the new firing angle is bounded (for example between 5° and 85°) to prevent switching misfires in Block E. With the new firing angle α_{next} and zero crossing time t_0 from DSP, Block F sequentially generates the firing pulses for six valves. The mathematical notation is as follow:

$$\text{Valve } k: \quad t_k = t_0 + t_{delay} + \frac{k}{(6f_0)} \qquad (22)$$

Where the time delay is calculated as $t_{delay} = (\alpha/360) \times T_0$, T_0 is fundamental period, f_0 is fundamental frequency, and k assumes integer values from 1 to 6.

The main idea of the digital controller for an inverter is very similar to the rectifier controller, and only the differences in firing delay angle has to be computed from the extinction angle (γ) as follows.

$$V_{di} = V_{d0i}\cos\gamma - K_{\Omega i}I_{di} \qquad (23)$$

$$\Delta V = -V_{d0i}\sin\gamma \cdot \Delta\gamma \qquad (24)$$

$$\Delta\gamma = \frac{\Delta V}{-V_{d0i}\sin\gamma} \qquad (25)$$

$$\Delta V = V_{ref} - V_{dc} \qquad (26)$$

$$\gamma_{next} = \gamma + \Delta\gamma \qquad (27)$$

$$\alpha_{next} = 180^0 - (\gamma_{next} + \mu) \qquad (28)$$

Where V_{di} is the measured direct voltage at the inverter side, V_{d0i} is no-load direct voltage at inverter, $K_{\Omega i}$ is equivalent commutation resistance, and μ is commutation angle.

III. COMPARISON OF TRAPEZOIDAL AND QUADRATIC INTEGRATION

A. Accuracy Comparison

Accuracy is an important characteristic of numerical integration methods, since the reliability of power transient analysis depends on it. In this paper, the accuracy of the quadratic integration is compared with that of the trapezoidal integration. The shaded parts of Fig.7 show symbolically and exaggerated the integration error of both methods, and the accuracy of solutions by the applications of both methods is depended on these integration errors.
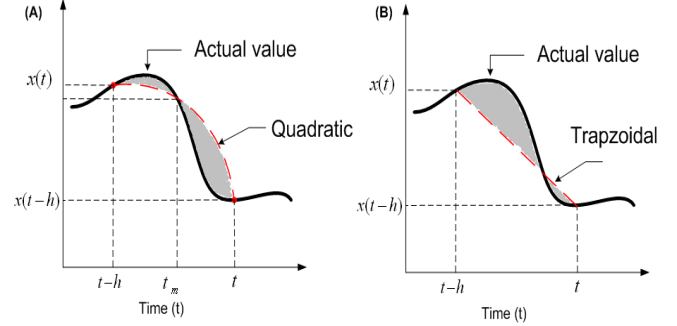

Fig. 7. Integration error of both methods.
((A) quadratic integration, and (B) trapezoidal integration)

The truncation error is represented as follows (since the trapezoidal integration is order two accurate and the quadratic integration is order four accurate [1]):

$E_{trapezoidal} = O(h^2)$ and $E_{quadratic} = O(h^4)$ over the interval [t-h, t], where E denotes the truncation error, and h is the time step. That is, the dominant error per step of trapezoidal integration is proportional to h^2 and that of the quadratic integration is proportional to h^4.

In order to demonstrate the increased accuracy of the quadratic integration method, a simple switching system is used as shown in Fig.8. The results by application of the trapezoidal and the quadratic integration methods are compared with the direct (analytical) solution. Specifically, the direct solution (exact solution) is calculated analytically (using Laplace transform).
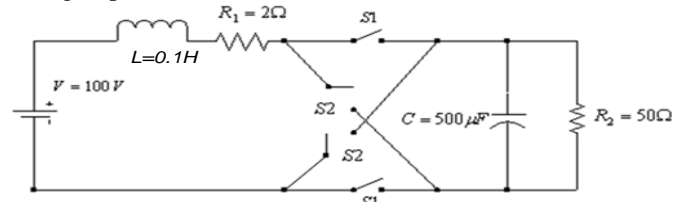

Fig. 8. A simple switching system

The switches shown are ideal electronic, and the sequence of switching given with: Switches S1 are closed at t=0.0T+kT, and opened at t=0.5T+kT, and switches S2 are reversely operated, where the switching period T is 0.02 seconds, and k is integer, 0, 1, 2, ... The model equations are:

S_1 is ON, and S_2 is OFF.

$$\begin{cases} L\dfrac{di_L(t)}{dt} = v(t) - v_c(t) - R_1 i_L(t) \\ C\dfrac{dv_c(t)}{dt} = i_c(t) \\ 0 = i_L(t) - \dfrac{v_c(t)}{R_2} - i_c(t) \end{cases}$$

S_1 *is OFF*, *and* S_2 *is ON*

$$\begin{cases} L\dfrac{di_L(t)}{dt} = v(t) + v_c(t) - R_1 i_L(t) \\ C\dfrac{dv_c(t)}{dt} = i_c(t) \\ 0 = i_L(t) + \dfrac{v_c(t)}{R_2} + i_c(t) \end{cases} \quad .$$

Fig.9 shows the results (inductor current and the capacitor voltage) from the direct analytical solution. The results by application of the trapezoidal and quadratic integration methods they appear to be similar in form as the waveforms of Fig.9. In order to show the error clearly, Fig 10 shows the absolute errors of both numerical methods during last 0.1 second and for two different integration time steps.
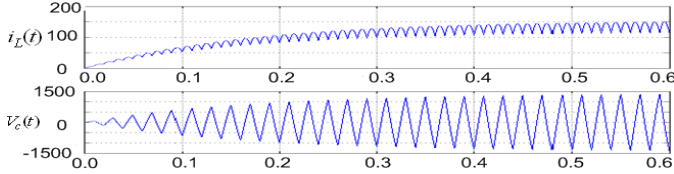
Fig. 9. Analytical simulation results
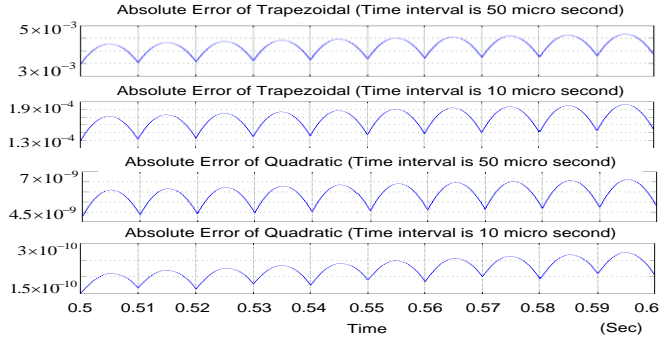
Fig. 10. Absolute error of the inductor current by both numerical methods in steady state

The absolute error is defined as:

$$error = \left| i_{actual}(t) - i_{numerical}(t) \right| \tag{29}$$

where i_{actual} is actual inductor current calculated by the Laplace transform, and $i_{numerical}$ is inductor current by applications of the trapezoidal and quadratic integration. Note that the absolute errors of the quadratic integration are about six orders of magnitude smaller than the errors of the trapezoidal integration. The example shows clearly the substantially higher accuracy of the quadratic integration method as compared to the trapezoidal integration. The computational cost of the quadratic integration is almost twice as much as that of the trapezoidal integration with the same time step. However, the quadratic integration with time step of 50 micro-seconds as compared to the trapezoidal integration with time step 10 microseconds offers more accurate simulation results (more than three orders of magnitude) at a fraction of the execution time (about 50% of the execution time of trapezoidal integration).

B. Numerical Oscillation Comparison

Power transient analysis by application of Trapezoidal integration has been suffered from numerical oscillations especially in systems with nonlinearities and switching subsystems. The root cause of the fictitious oscillations is well known. The accuracy of the trapezoidal and quadratic integration methods has been studied and reported in previous publications [1], [3]. The possibility of fictitious oscillatory solution can be studied from the general form of the numerical solution of simple dynamical systems. Consider for a example a first order dynamical system:

$$\frac{dx}{dt} = ax, \text{ where } a < 0. \tag{30}$$

The physical system is stable, since $a < 0$. Therefore the direct analytical solution is also stable. The numerical solution using trapezoidal integration is:

$$x(t) = \left(\frac{2+z}{2-z} \right) x(t-h), \text{ where } z = ah, \text{ and h is positive.} \tag{31}$$

If the integration time step is so selected as to $z < -2$, the numerical solution for $x(t)$ will oscillate around the true values. Because the method is absolutely stable, the true values can be approximated by filtering the oscillations. The numerical solution using the quadratic integration, after eliminating the mid-point, x_m, is:

$$x(t) = \left(\frac{12 + 6z + z^2}{12 - 6z + z^2} \right) x(t-h) \tag{32}$$

where $z = ah$, and h is positive.

Note that in the numerical solution (32) the coefficient cannot become negative for any selection of the integration time step (a is negative and h is positive). Therefore, the quadratic integration is free of fictitious oscillations as compared to the trapezoidal integration.

To demonstrate numerical oscillations graphically, the six pulse converter model of Fig.2 is simulated with three methods and with an appropriately selected integration time step (same for all methods): (a) purely trapezoidal integration, (b) trapezoidal integration with the numerical stabilizer method, and (c) purely quadratic integration. The results are shown in Fig.11.
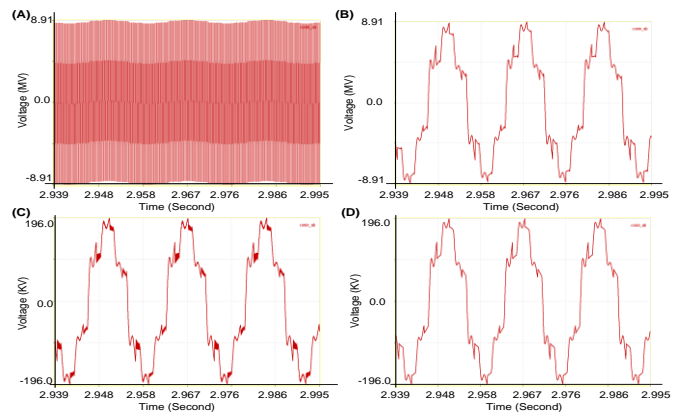

Fig. 11. Line-Line voltage between Phase A and phase B of the six-pulse converter. ((A) Purely trapezoidal, (B) Filtered waveform of (A), (C) Trapezoidal with numerical stabilizer, and (D) Quadratic integration)

Trace (A) is the Line-Line voltage (A-B) solution using the trapezoidal integration and trace B is the filtered version of this solution. The results clearly demonstrate the existence of fictitious oscillations around the true solution of the system. Trace (C) shows the solution when numerical stabilizers are

used in the trapezoidal integration. Trace (D) shows the solution by application of the quadratic integration which is free of fictitious oscillations.

IV. SIMULATION OF HVDC SYSTEM - EXAMPLE RESULTS

The quadratic integration method is demonstrated on a typical 12-pulse HVDC system. The demonstration example is shown in Fig.12. Each component of the system of Fig 12 is modeled with a set of nonlinear and differential equations derived directly from the physical parameters of the components.
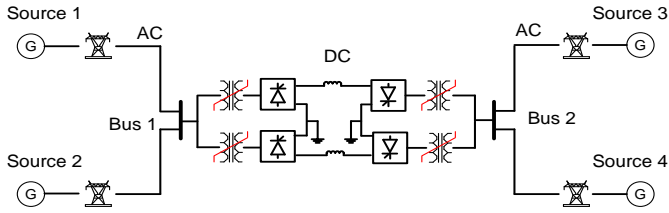

Fig. 12. A HVDC system for testing the properties of quadratic integration

TABLE III
SETTING VALUES OF PARAMETERS FOR THE 12-PULSE HVDC SYSTEM

Equivalent Source	Line-to-Line voltage (RMS)	225 kV
	Inductance (L)	10 mH
	Resistance (R)	5 Ω
the parameters of converters	Snubber (C_S)	0.1 uF
	Snubber (R_S)	1200 Ω
	Limiting (L)	10 mH
	Limiting (R)	3000 Ω
	Thyristor (C_P)	20 nF
	Thyrister($G_{V1} \sim G_{V6}$ of ON)	100 Mhos
	Thyrister($G_{V1} \sim G_{V6}$ of OFF)	0.1 uMhos
	Smoothing(C)	50 μF
DC-Line	Inductance (L)	0.1 H

The 12-pulse HVDC system consists of AC transmission lines, two 6-pulse rectifiers, two 6-pulse inverters, a DC transmission line, and four three phase saturable-core transformers. A total of four three-phase equivalent sources represent the rest of the system. The parameters of the major components of the system are shown in Table III. At steady state, the DC transmission line transmits total real power of 200 MW.
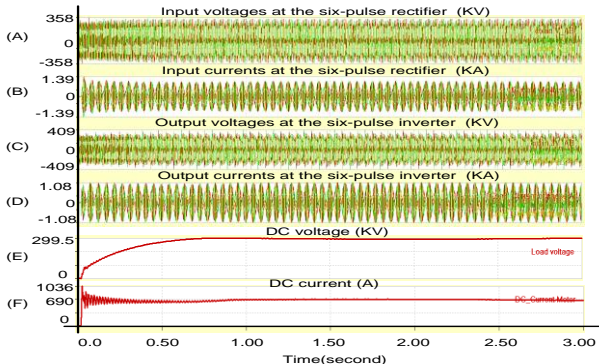

Fig. 12. (A) Input line-to-line voltages and (B) input currents before 6-pulse rectifier, (C) output line-to-line voltages and (D) output currents after 6-pulse inverter, and (E) DC voltage and (F) DC current.

Fig.12 shows the three phase voltages (A) and the three phase currents (B) at the input of the rectifier, the three phase voltages (C) and the three phase currents (D) at the output of the inverter, and the voltage (E) and current (F) of the DC Line. Fig.13 shows the same quantities zoomed into the time interval from 2.930 to 3.000 (seconds). Note that the voltages and currents exhibit the usual distortion incurred by the operation of the rectifier and inverter.
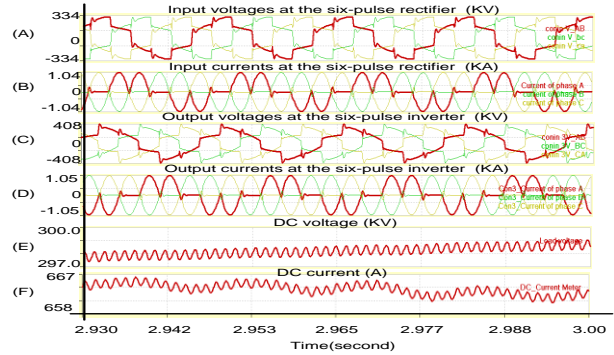

Fig. 13. (A) Input line-to-line voltages and (B) input currents before 6-pulse rectifier, (C) output line-to-line voltages and (D) output voltages after 6-pulse inverter, and (E) DC voltage and (F) DC current from 2.930 to 3.000 second.
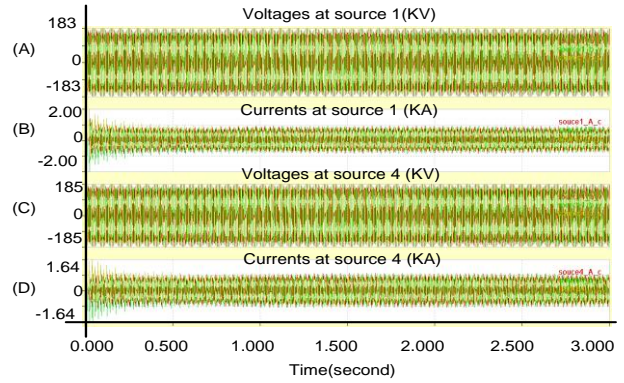

Fig. 14. (A) Three phase voltages and (B) currents at source 1, (C) three phase voltages and (D) currents at source 4.
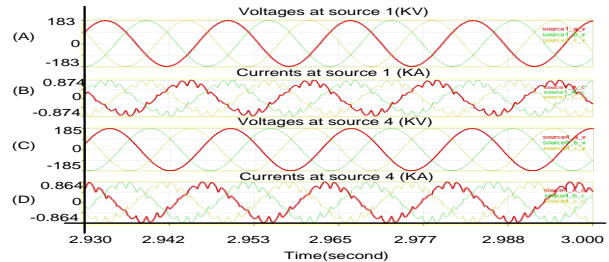

Fig. 15. (A) Three phase voltages and (B) currents at source 1, (C) three phase voltages and (D) currents at source 4 from 2.930 to 3.000 seconds.
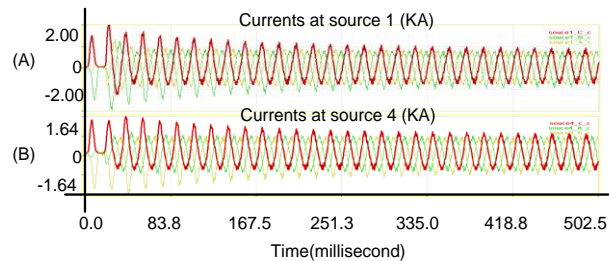

Fig. 16. (A) three phase currents at source 1, (B) three phase currents at source 4 from 0.0 to 502.5 milliseconds.

The graphs in Fig.14, 15 and 16 show (A) three phase voltages and (B) currents at source 1, (C) three phase voltages and (D) current at source 4. Close examination of the waveforms show the presence of inrush currents during the transient period which decay and become negligible at steady state. The shape of the current waveforms in Fig.15 are closer to sinusoidal as compared to the currents at the input of the rectifier or the output of the inverter as expected.

Another example is shown in Fig.17 and 18. In the example we simulate a HVDC transmission system in steady state and a step change order in power. Specifically, while the system was operating at 200 MW of transmission through the HVDC transmission line, a power change order of 100 MW (for a total of 300 MW) is provided at time 3.5 seconds. The response of the system is shown in the above mentioned figures. Note that DC current and voltage transit very fast to the new operating point. The firing angles (extinction angles, etc.) of the four 6-pulse converters are automatically regulated to meet the power order. In this simulation, we demonstrate that the system can respond very fast to the power order change. In real systems the power order will be in the form of a power ramp that will result in smoother transitions of the operating point.
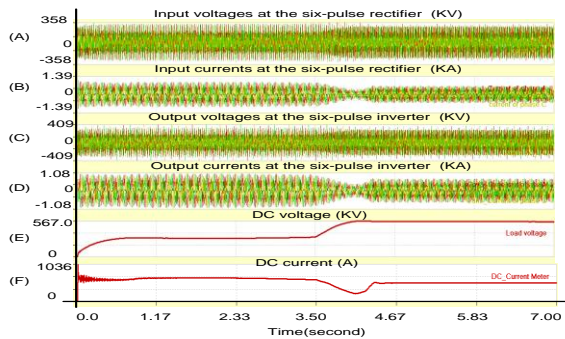

Fig. 17. (A) Input voltages and (B) input voltages before 6-pulse rectifier, (C) output voltages and (D) output voltages after 6-pulse inverter, and (E) DC voltage and (F) DC current.
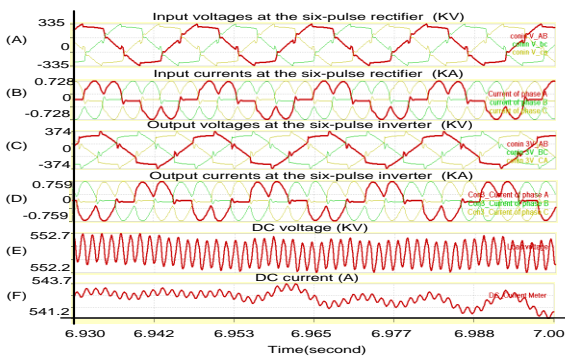

Fig. 18. (A) Input voltages and (B) input voltages before 6-pulse rectifier, (C) output voltages and (D) output voltages after 6-pulse inverter, and (E) DC voltage and (F) DC current from 2.930 to 3.000 second.

V. CONCLUSIONS

This paper presented an advanced time domain method and its application on a HVDC transmission system. The proposed quadratic integration method is order four accurate. Simulation results are more accurate than those by application of the trapezoidal integration method. The quadratic integration method eliminates fictitious oscillations, accurately models nonlinear subsystems such as saturable-core transformers and accurately models the operation of switching subsystems. The proposed method is well suited for high fidelity simulation of complex HVDC systems.

VI. REFERENCES

[1] A. Meliopoulos, G. Cokkinides, and G. Stefopoulos, "Quadratic integration method," in Proceedings of the 2005 International Power System Transients Conference (IPST 2005). Citeseer, pp. 19–23.

[2] M. Roitman and P. S. R. Diniz, "Simulation of non-linear and switching elements for transient analysis based on wave digital filters," IEEE Trans. on Power Delivery, vol. 11, no. 4, pp. 2042-2048, Oct. 1996.

[3] W. Gao, E. Solodovnik, R. Dougal, G. Cokkinides, and A. Meliopoulos, "Elimination of numerical oscillations in power system dynamic simulation," in Applied Power Electronics Conference and Exposition, 2003 APEC'03. Eighteenth Annual IEEE, vol. 2, 2003.

[4] J.Lin,J.R. Marti-"Implementation of the CDA Procedure in the EMTP"-IEEE Transaction on Power Systems, V.5, n.2,pp.394-402, May 90.

[5] S N Hong, C R Liu, Z Q Bo, and A Klimek, " Elimination of Numerical Oscillation of Dynamic Phasor in HVDC system Simulation," in Power and Energy Society General meeting,PES'09.IEEE,pp1-5,July 2009.

[6] M Roitman, P s R Diniz-" Power systems simulation based on Wave Digital filters" IEEELPES 1995 Summer Meeting, paper 95 SM 400-2 PWRD, Jul95.

[7] A.P.Sakis Meliopoulos, George J.Cokkinides, George. Stefopoulos, "Symbolic integration of dynamical systems by collocation methods," in Proc. 2005. IEEE Power Engineering Society General Meeting, Vol. 1 pp. 817 - 822.

[8] A. Ekstrom and G. Liss, "A refined HVDC control system," IEEE Transactions on Power Apparatus and Systems, pp. 723–732, 1970.

[9] R. Simard and V. Rajagopalan, "Economical Equidistant Pulse Firing Scheme for Thyristorized DC Drives," IEEE Transactions on Industrial Electronics and Control Instrumentation, pp. 425–429, 1975.

[10] S. Bhat, "Novel equidistant digital pulse firing schemes for three-phase thyristor converters," International Journal of Electronics, vol. 50, no. 3, pp. 175–182, 1981.

[11] J. Ainsworth, "The Phase-Locked Oscillator: A New Control System for Controlling Static Convertors," IEEE Transactions on Power Apparatus and Systems, pp. 859–865, 1968.

[12] N. Mohan, T. Undeland, and W. Robbins, Power electronics: converters, applications, and design. Wiley India, 2007.